

A. Information About the Proposal

A.1. Instrument Location and Type

Instrument location: National Center for Atmospheric Research (NCAR) High Altitude Observatory (HAO), Boulder, CO, USA

Instrument type: The Airborne Coronal Emission Surveyor (ACES) is an infrared (IR) imaging Fourier Transform Spectrometer (FTS), a type of optical instrumentation.

A.2. Justification for Submission as a Development Proposal

- How will the end result of the effort be a stable shared-use research instrument, rather than technology development, a device, a product or a technique/protocol?

We will validate and deliver a novel IR imaging spectrometer that can be used to quantify the intensity variations of strong coronal emission lines as a function of radius and solar features.

- What significant new capabilities, not available in an instrument provided by a vendor, will the new instrument provide?

The instrument will extend the capabilities of existing commercial single-pixel FTS designs to a design that produces a three dimensional spectral-image cube for each pointing.

- Does the instrument development effort build capacity for instrument development activities within an MRI submission-eligible organization(s)?

Yes, the proposal builds on recent work with IR cryogenic spectrometers and allows for continued development of our solar IR instrumentation group. An FTS is well suited for broad spectral coverage; adding spatial imaging is essential to capture the solar corona's structure.

- In what way does the instrument development require design and development work that must be undertaken or has been undertaken in-house, rather than through readily available/published designs found in the literature?

No commercial or published FTS meets the ACES requirements for imaging performance and sensitivity. We will work closely with Bruker to specify an FTS that works as a testbed for ACES, but our group will design, build, and test ACES itself.

- To what extent does the instrument development require/benefit from a team of scientists/engineers/technicians that bring a variety of skills to the project?

The development of ACES requires expertise in solar physics and optical, mechanical, and software engineering, all provided by Smithsonian Astrophysical Observatory (SAO) scientists and engineers.

- For what activities does the instrument development require a significant number of person-hours, more so than simple “assembly” of purchased parts?

The design, construction, alignment, and testing of the instrument are all labor intensive. ACES will integrate into our existing Airborne Stabilized Platform for IR Experiments (ASPIRE).

- To what extent does the instrument development require timeframes for completion that are longer than are required for plug-and-play or assembled instruments?

The components of ACES must be designed, manufactured, and assembled into an instrument, requiring longer timeframes than assembly of plug-and-play components. The fixed date of the solar eclipse (April 8, 2024) places strong constraints on the timeline. Our experience developing ASPIRE and our Airborne IR Spectrometer (AIR-Spec) has taught us how to ensure that the design, build, and flight testing proceed without complication.

- Does the instrument development require the use of a machine shop or a testbed to fabricate/test unique components?

Yes, we have budgeted machine shop time as part of our proposal.

- Does the instrument development effort involve risks in achieving the required specifications, and what is the risk mitigation plan?

The major risk is associated with achieving the required specifications in time for the eclipse. See Section E.3 for the risk mitigation plan.

B. Research Activities to be Enabled

ACES is a new instrument that uses the ASPIRE platform to explore the large-scale coronal IR emission spectrum during the 2024 total solar eclipse. ACES and ASPIRE will fly on the NSF/NCAR Gulfstream V High-performance Instrumented Airborne Platform for Environmental Research (GV HIAPER) along the path of totality during the second Great American Eclipse in 2024. ACES will use the 20 cm optical feed from ASPIRE to map emission line intensity as a function of radius and solar magnetic structure. The program builds on our experience developing airborne IR instrumentation, including AIR-Spec, a cryogenic IR spectrometer that observed the 2017 and 2019 eclipses, and ASPIRE, built and ground tested during the pandemic with GV test flights planned for spring 2021 and an eclipse validation flight in December 2021.

B.1. Results from Prior NSF Support

B.1.1. MRI: Development of an Airborne Infrared Spectrometer (AIR-Spec) for Coronal Emission Line Observation

Principal Investigator: Edward DeLuca, Co-Principal Investigator: Leon Golub

Award #1531549, Amount: \$1,200,591.00, Period of support: August 15, 2015–July 31, 2018

Intellectual Merit: During the 2017 total solar eclipse, AIR-Spec took a step toward the direct observation of coronal magnetic fields by measuring infrared emission in the solar corona from aboard GV HIAPER. The instrument successfully observed the five coronal emission lines that it was designed to measure, Si X 1.43 μm , S XI 1.92 μm , Fe IX 2.85 μm , Mg VIII 3.03 μm , and Si IX 3.93 μm , which were identified by Judge [15] as promising candidates for future spectropolarimetric observations based on abundance, charge state, branching ratios and collision destruction probabilities. Characterizing these magnetically sensitive emission lines is an important first step in developing the next generation of instrumentation to measure the coronal magnetic field. During the eclipse observation, AIR-Spec measured the average linewidths, peak intensities, and center wavelengths of all five lines radially outward from the limb at four positions in the corona. The observation of Fe IX at 2.85 μm was the first of that line [28].

AIR-Spec was designed as a cryogenic slit spectrometer that measured light over a $1.55 R_{\odot}$ field of view (FOV) in four spectral passbands between 1.4 and 4 μm . The original package included an image stabilization system (the first to fly on the GV), feed telescope, grating spectrometer housed in a cryogenic vacuum chamber, and slit-jaw imager. The instrument development encountered a number of engineering challenges, centered around maintaining adequate resolution and signal-to-noise ratio (SNR) in a compact and inexpensive package on a moving platform, all of which were met to enable a successful mission.

The AIR-Spec measurements validated models by Del Zanna & DeLuca [4] for the intensity of Si X and Si IX as a function of distance from the limb (Figure 1, left two panels). The fall-off in intensity probes the relative importance of collisional and radiative excitation [13]. The models in Figure 1 have not yet been tuned, but still match the measured data to within a factor of two. With ACES, we will expand this work to constrain atomic models for 14 coronal ions (Section B.2).

Coordinated observations between AIR-Spec and the Hinode Extreme Ultraviolet Spectrometer (EIS) were used to characterize the coronal plasma near the west limb [22]. Our emission measure (EM) loci

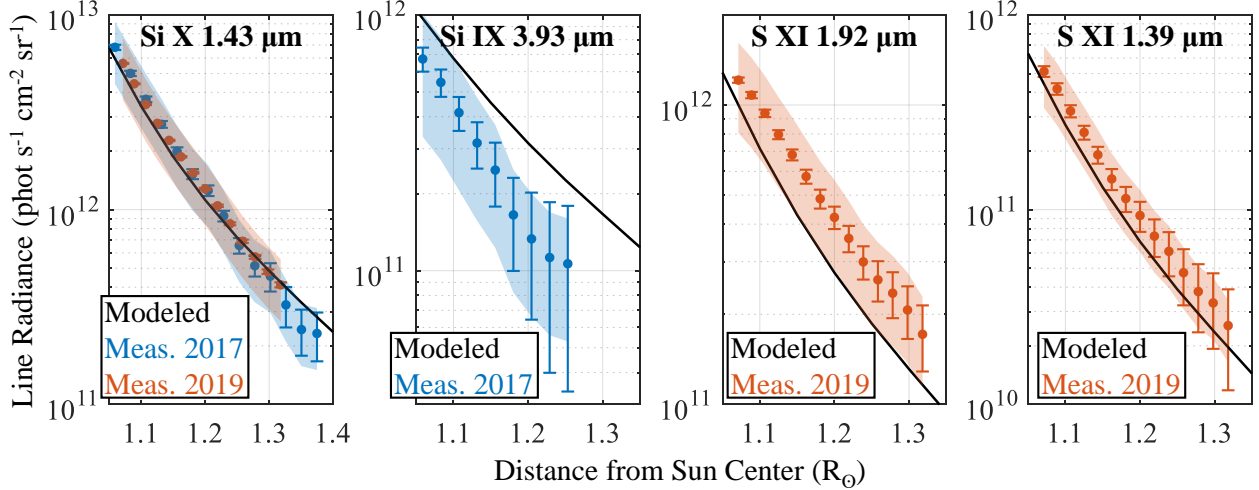


Figure 1. Line radiance vs. height, measured and modeled. The error bars represent 95% confidence intervals in the line fits. The shaded region spans two different radiometric calibrations, providing a measure of the calibration uncertainty.

analysis ratioed observed AIR-Spec line intensities to modeled volume emissivities to predict a temperature between $10^{6.0}$ and $10^{6.2}$ K (Figure 2), similar to the temperature found with EIS. Cooler plasma present in a prominence may explain why the Mg VIII ($T = 10^{5.9}$ K) curve intersects the others at lower temperature. ACES will measure at least 18 coronal lines, increasing the accuracy of future EM loci analyses.

Broader Impacts: The 2017 AIR-Spec mission provided training for students and early career researchers and a unique opportunity for public outreach before and after the eclipse. The AIR-Spec instrument scientist, Jenna Samra, was a Harvard PhD student who wrote her thesis on the instrument design and development, the data processing and calibration, and the first science results from the 2017 eclipse observation. The project allowed Vanessa Marquez, an early career engineer at SAO, to develop her mechanical and optical engineering skills as she took the lead role in the instrument’s mechanical design. Additionally, the project supported the training of a new postdoctoral fellow at SAO, Chad Madsen, who is now a full-time member of SAO’s research staff and a Co-PI on this proposal. In 2016 and 2017, the AIR-Spec team mentored three students in SAO’s Research Experience for Undergraduates (REU) program. All three students presented their work at meetings of the American Geophysical Union (AGU) [3, 34], the American Astronomical Society (AAS) [10], and/or the International Society for Optics and Photonics (SPIE) [35].

The 2017 eclipse mission was covered by the press and provided many opportunities for outreach. The project and team were featured in articles in *The New York Times*, *The Washington Post*, *Nature*, *Smithsonian Air & Space Magazine*, *Science News*, and *Forbes*. Outreach presentations were given to high school students at the Montrose School (Medfield, MA) and Blair Academy (Blairstown, NJ), undergraduates at Smith College, and the public at a meeting of the New England Section of the Optical Society of America.

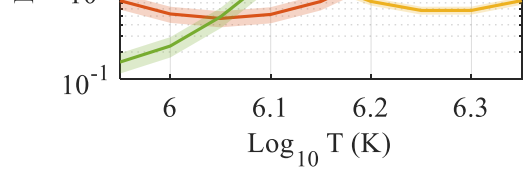


Figure 2. Using the observed AIR-Spec line intensities to estimate coronal temperature. The EM loci plot predicts a temperature between $10^{6.0}$ and $10^{6.2}$ K at the limb [22].

Publications: To date, AIR-Spec has resulted in four refereed publications [4, 28, 22, 14], two conference proceedings papers [27, 35], and over a dozen conference posters and presentations. The 2017 data is available online on the Virtual Solar Observatory.

B.1.2. Airborne InfraRed Spectrograph (AIR-Spec) 2019 Eclipse Flight

Principal Investigator: Edward DeLuca

Co-Principal Investigators: Peter Cheimets, Jenna Samra, and Vanessa Marquez Award #1822314, Amount: \$519,286.00, Period of support: May 15, 2018–April 30, 2021

Intellectual Merit: The second AIR-Spec research flight took place during the July 2, 2019 total solar eclipse over the south Pacific. Totality lasted for 9 minutes and produced 7 minutes of data in 9 slit positions. AIR-Spec pointed primarily at the east and west limbs, where models predicted the brightest intensity and where we had arranged for co-located observations with Hinode/EIS.

In the year leading up to the observation, AIR-Spec underwent significant upgrades to radically improve its sensitivity and image stability, and to correct two artifacts which appeared in the 2017 data. The IR camera manufacturer rebuilt the camera interface to remove light leaks, reducing the thermal background by a factor of 18 and removing its spatial structure. The upgrade resulted in more than four times higher SNR and significantly less error in the background subtraction. We added feedback to the image stabilization algorithm to reduce the root-mean-square (RMS) image motion by about a factor of six compared to the feedforward-only 2017 algorithm. The 2019 image stabilization system, which tracked the limb of the sun in the slit-jaw camera, was the basis for ASPIRE, which will deliver the ACES solar feed. We blocked stray reflections from the slit-jaw, which resulted in ghost images of the strong lines in the 2017 spectrum [29], and added mechanical constraints to the adjustable spectrometer mirrors to stop mirror vibration from distorting the lineshape. The improvements are evident in the example spectrum shown in Figure 3.

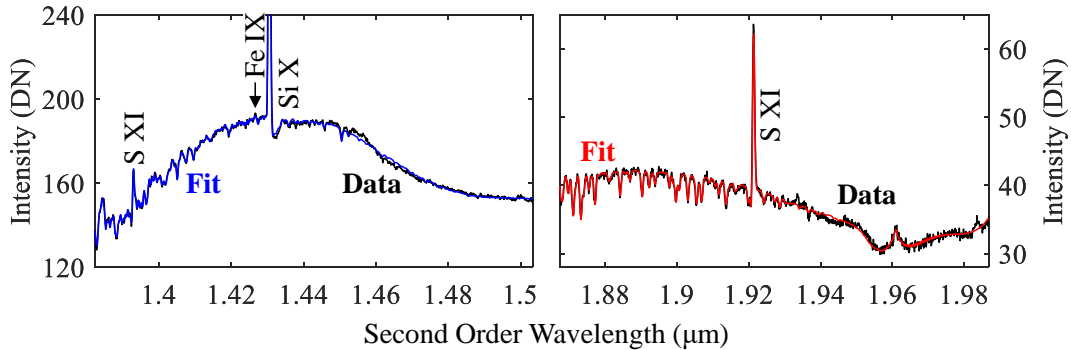


Figure 3. AIR-Spec measurement over 140 arcsec near the east limb, average of 436 frames at 0.25 second exposure time. The four target emission lines are labeled. An atmospheric model was used to extract accurate line intensities in the presence of significant telluric absorption, and fits are shown in blue and red.

Figure 3 shows the four emission lines observed by AIR-Spec in 2019. The $3.93\text{ }\mu\text{m}$ Si IX line was not observed because the long-wavelength cutoff was reduced as part of the background-reduction effort, and the $3.03\text{ }\mu\text{m}$ Mg VIII line was not observed because the passband was tuned to observe the $1.39\text{ }\mu\text{m}$ line of S XI instead. The S XI line was chosen because it is half of a density-sensitive line pair and was unobserved at the time of the 2019 eclipse. Significant (5–10%) atmospheric absorption was measured near the emission lines, and atmospheric modeling was required to extract accurate line intensities (blue and red curves in Figure 3). The atmospheric structure help us precisely calibrate the wavelength and instrument line shape and provided a check on the radiometric calibration, given some assumptions about the continuum

brightness. In the short-wavelength channel, it provided a way of separating the first and second-order continuum, as the absorption features only showed up in one order or the other.

Si X and S XI line intensities are plotted as a function of radial distance in panels 1, 3, and 4 of Figure 1. The improved sensitivity over the 2017 observations is evident in the much smaller error bars in the Si X fits. The measured and modeled intensity fall-off agree extremely well, implying that the relative contributions of radiative and collisional line excitation are well understood.

The density-sensitive S XI line pair was used to measure the plane-of-sky (POS) density up to $0.35 R_{\odot}$ above the east limb (Figure 4). The S XI line emission has significant contributions from photoexcitation, and is therefore not restricted to the POS. Before the line ratio was taken, the line intensities were corrected for line-of-sight (LOS) effects

using the model shown in Figure 1. Measured intensities were scaled by the modeled fraction of light coming from within 24 arcsec of the POS. The resulting AIR-Spec density closely matches the modeled density as well as polarized brightness (pB) measurements from a ground-based camera deployed by HAO.

Broader Impacts: The 2019 AIR-Spec re-flight provided research projects for two more SAO REU students. Our 2018 summer student assisted with the image stabilization system upgrade and presented her work at the 2018 AGU Fall Meeting [25]. Our 2019 REU student, Naylynn Tañón Reyes, traveled to the eclipse operations base in Peru with the AIR-Spec team to do outreach in Spanish. She gave an AIR-Spec talk at Instituto Nacional de Investigación y Capacitación de Telecomunicaciones (INICTEL) on the campus of Universidad Nacional de Ingeniería and a tour of the GV aircraft and AIR-Spec instrument to the local press and visiting professors [32]. After the eclipse, she completed a science project [33] using AIR-Spec data. The 2019 eclipse mission was featured in an NCAR press release and articles in *Forbes* and *El Comercio*.

Publications: Two publications are currently in progress on the 2019 instrument and observations and the coordinated density diagnostics from AIR-Spec, EIS, and the HAO PolarCam.

B.1.3. MRI: Development of an Airborne Stabilized Platform for InfraRed Experiments (ASPIRE)

Principal Investigator: Jenna Samra

Co-Principal Investigators: Edward DeLuca, Peter Cheimets, and Vanessa Marquez

Award #1919809, Amount: \$697,975.00, Period of support: August 15, 2019–July 31, 2022

Intellectual Merit: ASPIRE is an extension of the successful AIR-Spec missions to the 2017 and 2019 total eclipses. The AIR-Spec optical feed was developed for the 2017 solar eclipse over the United States and underwent extensive modification to accommodate the elevation angle and location of the 2019 eclipse over the southeastern Pacific. The stabilization mirror used in both eclipses restricted the collecting optics to 10 cm diameter. ASPIRE is a versatile platform that can observe the sun at a range of elevation angles and locations with a minimum of customization. It delivers a 20 cm beam stabilized to 5 arcsec RMS, providing four times the geometric area of its predecessor and reducing the development time for new focal plane instruments by removing the burden of image stabilization.

Image stabilization is provided by a 30 cm gimballed steering mirror, gyroscope, and dedicated high-speed visible light camera. A periscope adapts the beam height to the focal plane instruments. During its commissioning flight, ASPIRE will feed two first-light instruments: AIR-Spec with a new larger telescope,

and a new multi-thermal narrowband imager in Si X and S XI. In future flights, the image stabilization system (mirror, gyro, and camera) will be reflown with new focal plane instruments. Figure 5 shows ASPIRE and its first-light instruments in the laboratory at SAO.

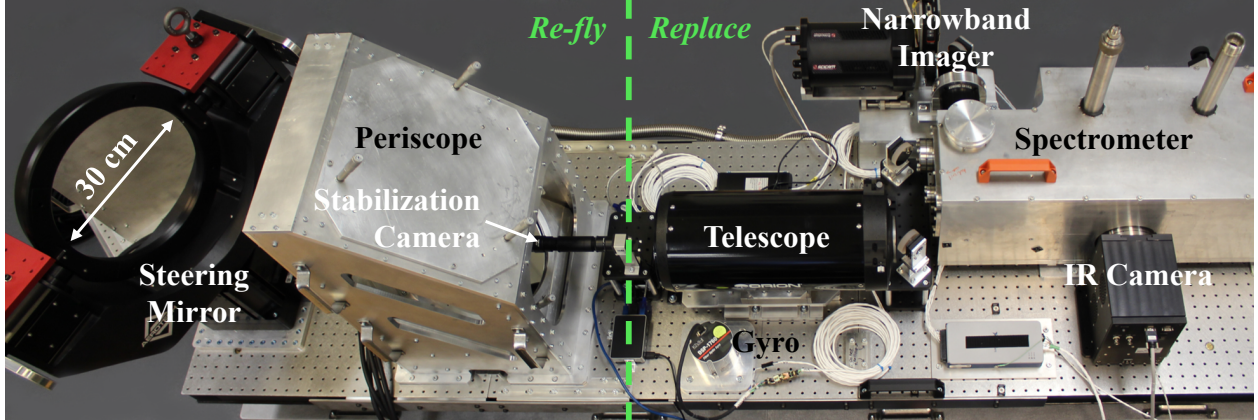


Figure 5. ASPIRE and commissioning focal plane instruments in the laboratory at SAO.

ASPIRE was originally scheduled to be commissioned during the December 14, 2020 total eclipse over South America, but the deployment was cancelled due to the COVID-19 pandemic. The commissioning flight is now scheduled for the December 4, 2021 eclipse over Antarctica, with test flights out of Broomfield, CO planned for spring 2021. ASPIRE's flexibility is demonstrated by the fact that the platform was configured to track the 2020 eclipse at 73° elevation and needs only to be moved across the aisle to track the 2021 eclipse at 17° elevation.

ASPIRE and its two first-light focal plane instruments have been assembled, aligned, and thoroughly tested in the laboratory. After alignment, the new telescope was shown to be nearly diffraction-limited at 633 nm. The narrowband imager works as expected, and the spectral focus and thermal background of the spectrometer are unchanged from the 2019 eclipse. The new image stabilization camera reliably delivers frames at 100 Hz, and the new mirror meets its specified bandwidth requirements.

We have developed a new image stabilization algorithm (Figure 6) which improves on the 2019 algorithm in three ways: it compensates for the 4 ms gyroscope delay, it corrects for low-frequency gyro drift using the aircraft's inertial navigation system, and it compensates for the mirror transfer function to improve the speed of the response. A simulation of the system predicts that it will stabilize the image to 1–2 arcsec RMS in the presence of a disturbance equal to the aircraft roll during the 2019 eclipse (Figure 7). Based on this model, laboratory testing, and the success of its prototype during the 2017 and 2019 eclipses, we expect the upcoming test flights to demonstrate that ASPIRE meets the 5 arcsec RMS stabilization requirement with margin.

Broader Impacts: ASPIRE provided opportunities for public outreach presentations to the Amateur Telescope Makers of Boston and the Smithsonian volunteer network. We had planned to have an REU student help build and align ASPIRE in summer 2020, but the REU program went virtual due to the pandemic and our student rescinded his acceptance. In summer 2021, our (most likely remotely based) REU student will analyze the optical performance of the new multi-thermal narrowband imager and predict the eclipse observations based on data we collect in the lab. Pandemic permitting, we will bring our former REU student Naylynn Tañón Reyes to our 2021 eclipse operations base in Punta Arenas, Chile to do Spanish-language solar physics outreach with the local community.

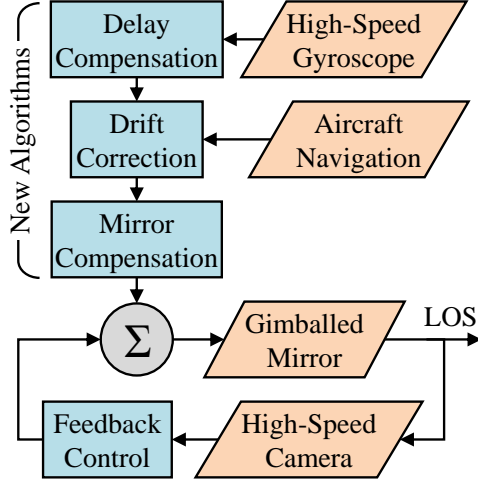


Figure 6. ASPIRE image stabilization block diagram.

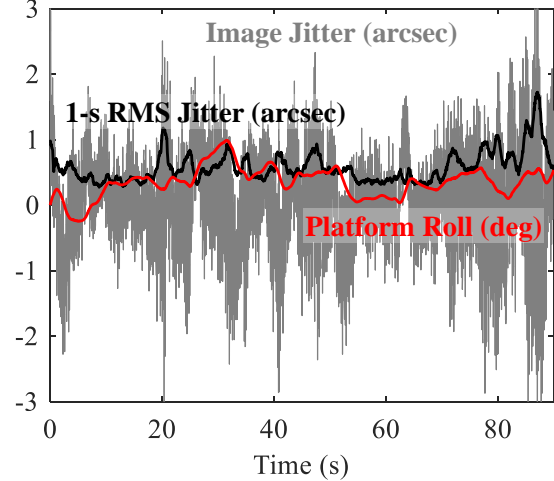


Figure 7. Predicted performance of the ASPIRE image stabilization system. The y-axis is in both arcseconds and degrees.

B.2. Proposed Investigation

AIR-Spec observed a narrow range of wavelengths and imaged along only one dimension. Now, we propose to expand our IR coronal program by surveying the entire 1–4 μm spectral range at high spectral resolution and in two spatial dimensions as a function of solar conditions and radius. ACES, our new imaging FTS, will search for lines that are viable candidates for measuring the coronal magnetic field and plasma diagnostics at large solar radii. It will be commissioned during the April 8, 2024 North American eclipse from GV HIAPER, with a solar feed provided by ASPIRE. A GV altitude of up to 14 km will enable ACES to survey the near and mid-IR with minimal atmospheric interference. ACES is expected to observe neutral helium as well as 18 forbidden lines of ionized magnesium, silicon, sulfur, argon, calcium, and iron (Table 1), and it may measure weaker lines of those and other ions. The eclipse mission addresses four science questions:

Q1. What are the strongest IR emission lines in different parts of the corona?

The formation of the He I 1083.3 nm triplet in the corona is complex and not well understood [6]. At low heights, it is comparable in strength to the nearby Fe XIII 1074.9 nm and 1081.1 nm lines [18, 19]. High-sensitivity maps of He I and the two Fe XIII lines will help untangle the formation processes. With strong emission lines from $\log T = 5.6 - 6.5$ K, we can identify the best lines to study the coronal hole boundaries at large solar radii. This is critical for understanding the corona/heliosphere interface and forecasting the propagation of eruptive events through the low corona [16, 17, 36].

Q2. What is the relative radiative to collisional excitation in each line as a function of radius?

IR emission lines arising from forbidden transitions are highly sensitive to electron collisions, but unlike UV emission lines, they are also influenced by photoexcitation from photospheric continuum radiation. Given the rarity of IR coronal observations up to the present day, the effects of photoexcitation in the corona remain vastly understudied. Quantifying the relative contributions of photoexcitation and electron collisions, given their intrinsic relationships to other atomic processes, is a critical check on theoretical atomic physics models such as those used by the CHIANTI atomic database [7]. This is achievable by comparing the radial fall-off of line radiance with that of electron density. In a purely collisional system, line radiance will fall off proportional to the square of electron density, while a purely photoexcited system will result in a linear dependence upon electron density. So, the relative contribution of the two

processes can be diagnosed by measuring the exponential dependence of line radiance upon electron density. As shown in Figure 1, the 2017 and 2019 AIR-Spec observations produced cursory results comparing radial radiance profiles of the strongest lines to theoretical profiles constructed using the collisional and photoexcitation models implemented by CHIANTI [7]. ACES will greatly expand upon this work with its larger number and variety of lines as well as its improved sensitivity.

Q3. What are the best temperature and density diagnostics in this passband?

The large variety of lines expected to be observed by ACES will open several diagnostic options for coronal plasma characterization. Of particular importance are line-ratio electron density diagnostics [e.g. 5]. We expect to observe four same-species line pairs with sensitivity across a range of electron densities typical of coronal plasma (highlighted in Table 1). The line pairs represent a wide range of formation temperatures from $\log T = 5.90 - 6.25$ K, ensuring testable density diagnostics for both quiescent and more active plasma. Furthermore, two of these pairs contain lines (Fe IX 2218.3 nm and Si IX 2584.6 nm) that have not been observed before according to [4], expanding the discovery potential of the mission. Unlike extreme ultraviolet (EUV) diagnostics, IR line-ratio diagnostics can suffer uncertainties propagated from poorly understood local photoexcitation and temperature effects. ACES will help diagnose these by providing four distinct yet simultaneous line-pair measurements. ACES will also expand upon line-ratio diagnostics of plasma temperature under conditions of ionization equilibrium by observing 14 possible combinations of lines arising from the same atomic element with different ionization states. The diversity of ion species observed by ACES will greatly facilitate additional temperature diagnostics, notably the EM loci method [e.g. 20, 22]. However, this diagnostic method requires precise knowledge of local elemental abundances in coronal plasma, which leads us to our final science question.

Q4. How do elemental abundances vary across the corona?

ACES will allow for the measurement of absolute elemental abundances in the corona, a crucial measurement for many spectroscopic diagnostics and for understanding the connectivity of the corona to the heliosphere. This will be possible since ACES will provide simultaneous observations of a large variety of emission lines as well as the scattered continuum arising from Thompson scattering of free electrons in the corona. The measurement strategy follows that first described by [38] and later adapted for observations of visible coronal emission during total solar eclipses [24, 23]. For this technique, the ratio of the total number of atoms of a particular element over the total number of electrons in the line of sight is isolated from the observed ratio of line and scattered continuum radiances. Unlike [38], we will be able take full advantage of the latest version of the CHIANTI atomic physics database [7], allowing us to avoid many of the

λ (nm)	Ion	LogT (K)	FIP (eV)	Fit Error (%)	QS	AR
1014.3	Ar XIII*	6.45	15.76		5.1	
1030.1	S XIII*	6.40	10.36		16.9	
1074.9	Fe XIII	6.25	7.90	0.7	0.3	
1080.1	Fe XIII	6.25	7.90	0.8	0.5	
1083.3	He I	4.50	24.59	4.9	6.3	
1252.4	S IX	6.05	10.36		12.7	
1392.8	S XI	6.25	10.36	22.5	4.0	
1430.5	Si X	6.15	8.15	1.1	0.8	
1920.1	S XI	6.25	10.36	11.7	3.2	
1935.0	Si XI*	6.20	8.15	20.8	10.0	
1963.0	Si VI*	5.60	8.15	6.7		
2206.3	Fe XII*	6.20	7.90	6.9	8.3	
2218.3	Fe IX*	5.90	7.90	9.5	17.2	
2265.0	Ca XIII*	6.50	6.11		14.2	
2482.6	Si VII*	5.80	8.15	3.2	15.0	
2584.6	Si IX*	6.05	8.15	5.3	5.9	
2856.3	Fe IX	5.90	7.90	7.9	17.3	
3028.5	Mg VIII	5.90	7.65	3.2	12.8	
3927.7	Si IX	6.05	8.15	5.3	12.1	

Table 1. Strong lines in the 1–4 μm range. Density sensitive line pairs and high-FIP elements are highlighted. Asterisks indicate lines that have not been observed [4]. The last two columns give the uncertainty (due to photon noise) in the measured line intensity at 1.1 R_\odot in the quiet sun (QS) and an active region (AR).

unphysical assumptions imposed by [38]. The broad wavelength range of ACES will enable simultaneous abundance measurements across seven elemental species: Ar, S, Fe, He, Si, Ca, and Mg. These elements cover a wide range of first ionization potential (FIP) as shown in Table 1, allowing us to better constrain the poorly understood FIP bias [e.g. 11, 8, 26] wherein, under most quiescent conditions, elements of low FIP are overrepresented in the corona when compared to photospheric abundances. The scientific literature contains a wealth of robust photospheric abundance measurements [e.g. 1, 31, 30]; however, it is currently not possible to meaningfully extrapolate these measurements to higher altitudes with a well-constrained radial model of the FIP bias. The wide FOV and broad spectral sensitivity of ACES will shed light on this issue with unprecedented measurements of the radial FIP bias dependence at multiple pointings out to $2 R_{\odot}$.

These science questions set requirements on the ACES design and implementation, which are addressed in Sections C.1 and C.2, respectively.

- A wavelength range of 1–4 μm is required in order to capture the strong Fe XIII line pair at 1.07/1.08 μm and the Si IX line at 3.93 μm , as well as at least 15 other coronal forbidden lines and a He I triplet.
- The spectral resolution must provide at least three samples across the width of the narrowest emission line for high-accuracy line fits.
- The FOV must sample different coronal conditions with one position due to the limited 6 minute duration of totality.
- The spatial resolution must be sufficient to distinguish between different coronal features.
- The sensitivity must be equal to or better than AIR-Spec, i.e. $\sim 1\%$ error in the fitted intensity of the strongest lines at $1.1 R_{\odot}$. From our previous measurements and models (see Figure 1), we expect that this will allow us to detect the strongest lines up to at least $2 R_{\odot}$ from disk center. Extrapolation of the ACES observations will set sensitivity requirements for future instruments that measure temperature and density further from the limb.
- Excellent radiometric calibration across the passband is required, as relative line intensities are critical for achieving the temperature, density, and differential emission measure (DEM) data sets.
- Pointing context is required to simplify the co-alignment of observations from ACES and other telescopes. A high-SNR context image will be obtained by integrating the ACES data cube across the wavelength dimension.

The ACES science team consists of the PI, two Co-PIs and our UK collaborator. Dr. Samra has responsibility for the overall management and direction of the science team. Dr. Madsen will lead the calibration effort and the development of the basic plasma data products: temperature ratios, EM loci maps and DEM analyses, density ratios, and absolute abundance determinations. Dr. DeLuca will lead efforts to coordinate with other eclipse experiments by ground-based and space-based solar observatories. We expect the ACES data products to be in high demand by groups studying the eclipse corona at higher resolution with more limited plasma diagnostics. Dr. Del Zanna will ensure that the appropriate underlying atomic physics is used in the analysis. He will work with Dr. Madsen on the data pipeline, providing comparisons with longstanding EUV observations from EIS and new spectroscopy from Solar Orbiter. The ACES team has close and longstanding research collaborations with scientists at NCAR. The concept of flying an FTS was discussed with Drs. Judge and Hannigan at NCAR ahead of the 2017 eclipse [14]. We will continue our collaborations with the NCAR team and coordinate with their eclipse plans.

C. Description of the Research Instrument and Needs

ACES was designed to meet the measurement requirements in Section B.2. Table 2 shows a list of optical specifications. As a Fourier transform spectrometer, ACES measures a wide range of wavelengths with high

spectral resolution. Imaging optics and a 2D detector provide sufficient FOV and spatial resolution to avoid repointing the instrument. ASPIRE provides the large-diameter, stabilized solar feed necessary to satisfy the sensitivity requirements. The ACES design and performance is described in Section C.1, and the development and testing is described in Section C.2.

C.1. Design and Performance

ACES consists of a condenser telescope and a Michelson interferometer (Figure 8). The condenser is a Gregorian telescope which provides a 5x compression of the beam. The beam exits the condenser to the side, allowing the central obscuration to be kept as small as possible, and enters the vacuum chamber that houses the interferometer. The interferometer has a fixed mirror, a scanning mirror, and a beamsplitter to send light to each mirror and recombine the beams that return. After the two paths recombine, the light is focused onto the IR detector by an achromatic triplet made of CaF₂ and sapphire.

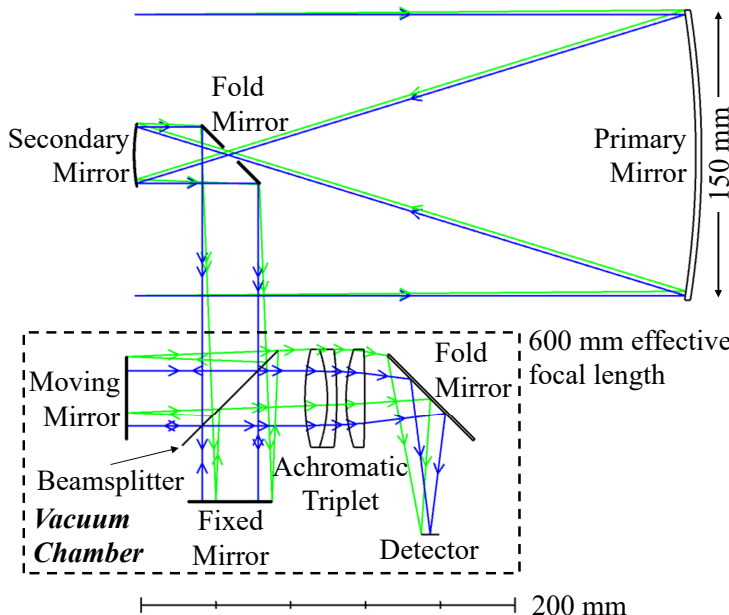


Figure 8. Ray trace of the ACES optical system.

formed at high resolution and inverse Fourier transformed to interferogram space, and the interferogram was truncated to reflect the ACES scan length and Fourier transformed back to wavenumber space.

The design in Figure 8 provides the optical performance shown in Table 2, satisfying the requirements listed in Section B.2. Figure 10 shows the spot diagrams at wavelengths across the passband, on-axis and in the corner of the image, at ZPD and \pm MPD. The spots are Nyquist-limited across the FOV, with an RMS diameter of about 8.5 arcsec near the center of the FOV and 13 arcsec in the corner. Figure 11 simulates the ZPD slice through the interferogram cube. The $0.73^\circ \times 0.55^\circ$ FOV is centered on an active region but encompasses regions of quiet sun and polar coronal holes, as well. Figure 12 shows the $3.9\text{ }\mu\text{m}$ (2546 cm^{-1}) Si IX line measured by ACES, with 3.5 samples across the linewidth. Because thermal linewidth increases with frequency, this is the narrowest line in the passband. Shorter wavelength lines will be better sampled.

Wavelength range	1–4 μm
Spectral resolution	0.2 cm^{-1}
Field of view	$0.73^\circ \times 0.55^\circ$
Plate scale	8.25 arcsec/pixel
Sensitivity	< 1% intensity error

Table 2. Optical performance.

The moving mirror changes the optical path difference (OPD) between the two legs of the interferometer, modulating the fringe pattern at the detector. As the mirror is scanned from zero path difference (ZPD) to maximum path difference (MPD), the interferometer sweeps out a three-dimensional (spatial \times spatial \times OPD) image cube, with an interferogram at each spatial pixel. Fourier transforming each interferogram produces a spectrum at each pixel. Figure 9 shows a simulated ACES interferogram and the corresponding spectrum at a pixel $1.1 R_\odot$ from sun center, in the absence of photon noise. To simulate the interferogram and spectrum, we used line intensities from [4], a continuum level of 10^{-6} times the brightness of the solar disk, and a model of the atmospheric absorption spectrum from an altitude of 14.3 km [21]. The spectrum was

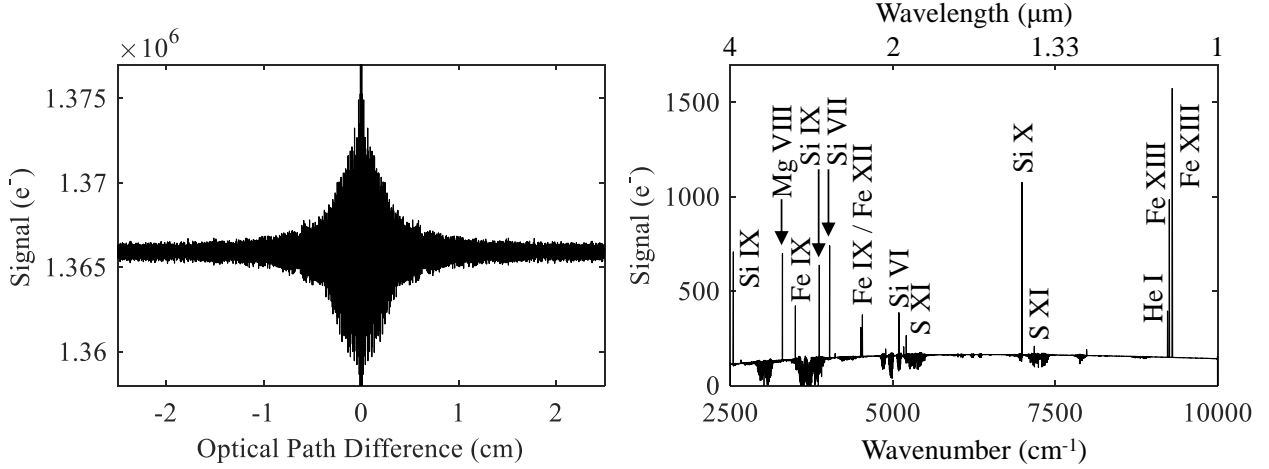


Figure 9. Modeled ACES interferogram (left) and spectrum (right).

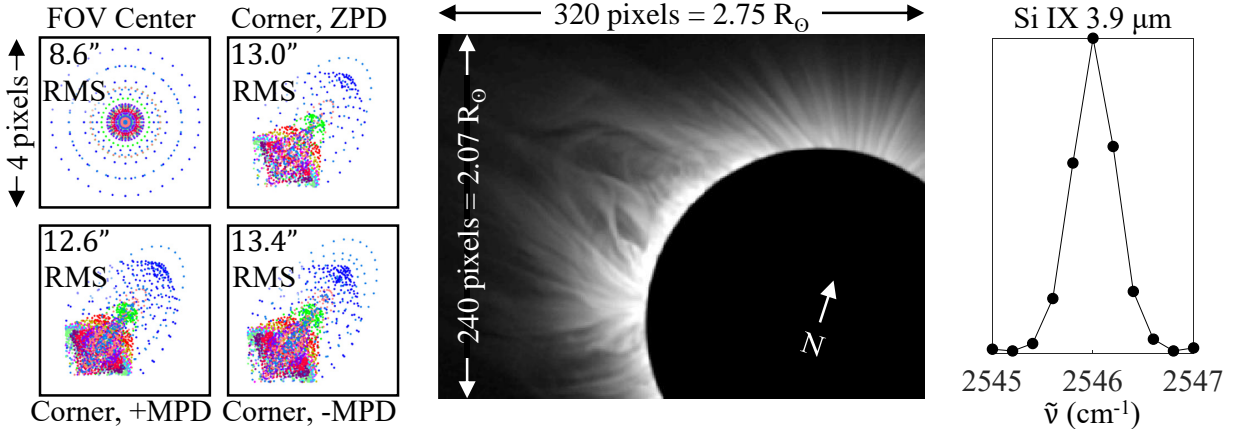


Figure 10. Spot diagrams and RMS diameters, 1–4 μm range.

Figure 11. Example image at ZPD, showing the FOV and spatial resolution.

Figure 12. Spectral sampling at 3.9 μm .

Table 3 lists the instrument specifications that result in the optical performance in Table 2. The spectral resolution requirement sets the scan length, and we sample the optical path difference at half of a HeNe wavelength in order to avoid aliasing the high-frequency (1 μm) end of the spectrum. The scan time is set by the length of the eclipse, about 6 minutes in the GV. Together, these parameters fix the scan speed and the number of exposures in the interferogram, which in turn set the required frame rate and exposure time.

The sensitivity requirement drives the aperture size, optical efficiency, thermal background (cryostat temperature), dark current (focal plane temperature), and detector material. We have selected an InSb detector from IR Cameras with 1280×1024 12 μm pixels and well depth, quantum efficiency, and dark current that meet our needs. To provide the required frame rate, the camera is windowed to 640×480 . To match the optical resolution and improve SNR, we bin 2×2 native pixels. A focal length of 600 mm gives the resulting 8.25 arcsec pixel size, which is small enough that the spectral resolution is not limited by the divergence in a pixel. This holds true as long as each pixel subtends an angle of less than $\alpha_{max} = \sqrt{\Delta\nu/\nu_{max}}$ [2, 12]. For ACES, $\alpha_{max} = 184.5$ arcsec.

In order to model the instrument sensitivity, photon noise was added to the “measured” interferograms before Fourier transforming, and Gaussian fits were performed on the noisy emission lines. Detector dark current and thermal emission from the interferometer optics contribute a constant background to the interferogram, but at a focal plane temperature of 70 K and an optics temp of 223 K, the dominant contributor to the noise is the interferogram itself. A 150 mm diameter aperture and optical efficiency of 0.4 (which includes a factor of 0.5 for the beamsplitter) results in very accurate fits to a number of strong lines. The last two columns in Table 1 list the predicted uncertainties in the fitted line intensity in the quiet sun and an active region.

C.2. Development and Testing

Before developing ACES, we will purchase a commercially available Bruker FTS with similar spectral range and resolution, a single-pixel detector, and room-temperature optics. The commercial FTS will serve as a testbed for the ACES development. By comparing ground-based and airborne solar observations from the Bruker FTS with photospheric spectral atlases [e.g. 9, 37] and atmospheric models [e.g. 21], we will quantify the errors in the measured interferograms and examine their relationship to aircraft vibration. Once we understand the data from the commercial FTS, we will use our findings to finalize the ACES optical design and mechanical/thermal implementation.

Our baseline implementation is shown in Figure 13. We will house the interferometer in a vacuum chamber and cool it to 223 K in order to minimize the thermal background, and we will coat the lenses and beam-splitter faces with anti-reflection coatings in order to maximize effective area. The KBr beamsplitter removes half of the light, but we will select telescope and interferometer mirrors with at least 98% reflectivity in the passband, resulting in an overall efficiency around 0.4. This is sufficient to ensure that the photon noise is

dominated by light from the corona and not the thermal background. We have chosen corner cube mirrors for the interferometer in order to ensure that the beam from the scanning mirror remains at a fixed angle as the mirror moves. This relaxes the requirements on the mirror drive mechanism and allows the use of larger diameter mirrors without resulting in degraded spectral resolution due to loss of fringe modulation [12].

ACES will be aligned in three steps. The condenser telescope will be aligned using the same Zygo interferometer and procedure that was used to align the original AIR-Spec telescope. The ACES interferometer will be aligned by adjusting the fixed mirror until its angle with respect to the beamsplitter is the same as that of the moving mirror (i.e. the signal at ZPD is maximized and the interferogram is symmetric) [12]. A collimator will be used to align the two subsystems to each other.

ACES will be calibrated on the ground and in flight. On the ground, wavelengths from 1 to 2.5 μm will be ra-

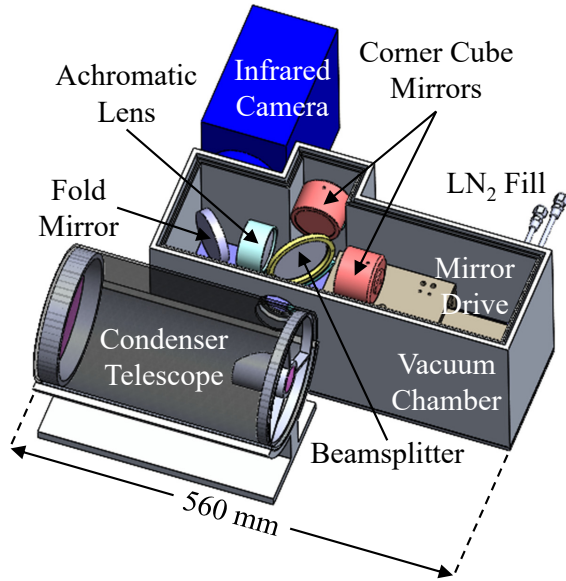


Figure 13. Mechanical and thermal implementation of ACES.

Scan length	± 2.5 cm
Sampling interval	316.5 nm
Scan time (2-sided)	360 s
Scan speed	0.140 mm/s
Exposure time	2.28 ms
Frame rate	439 Hz
Aperture diameter	150 mm
Focal length	600 mm
Optical efficiency	0.4
Cryostat temperature	223 K
Focal plane temp	70 K
Detector material	InSb
Focal plane format	320×240
Binned pixel size	24 μm

Table 3. Instrument specifications.

diometrically calibrated with an integrating sphere and wavelengths from 2.5 to 4 μm will be radiometrically calibrated with a thermal blackbody source. Calibration scans of the solar photosphere will be taken in flight before and after totality. The photosphere will be observed through a solar filter, and the filter transmission will be measured precisely in the laboratory. Wavenumber will be calibrated on the ground with emission lamps and in flight using the atmospheric absorption lines in the continuum.

After alignment and calibration is complete, ACES will undergo extensive testing on the ground in Cambridge, MA and Broomfield, CO and aboard the GV. Its performance will be validated using the same spectral atlases used to validate the Bruker FTS. In addition, the commercial FTS will serve as a comparison standard for ACES. After the flight tests are complete, we will assess the instrument's performance and make any modifications necessary for it to meet requirements ahead of the eclipse observation. Schedule details are provided in Section E.2.

D. Broader Impacts

New Research Infrastructure: After commissioning, ACES will be delivered to NCAR HAO, where it will be a valuable resource for the solar physics community. Due to its modular design, ACES can be repurposed for ground-based coronagraphic observations in addition to being flown in other eclipses. High-altitude studies with ACES may reveal new candidate emission lines for next-generation balloon- and space-borne instrumentation. Ground-based observations could be used to determine the practicality of observing particular lines in the presence of variable atmospheric transmission.

Student Education and Research Training: SAO has a strong REU program in solar physics, and REU students have been involved in all stages of the AIR-Spec development. ACES will provide research training for at least three more students over the lifetime of the project. Test flights in summer 2022 will provide field testing experience in Broomfield, CO. Our 2023 student will gain experience in optical alignment and calibration as we build ACES in the laboratory. In 2024, our student will analyze the recent eclipse observations and contribute to our papers in preparation.

Public Engagement with Science and Technology: Our previous eclipse missions have taught us that combining a total solar eclipse with the NSF GV is an excellent way to capture the public's attention. Based on our experience leading up to the last North American eclipse, we expect significant interest from the press and general public. The 2019 South American eclipse gave us the opportunity to do solar physics outreach in Spanish, and we will build on that foundation in 2024 with outreach events in both the US and Mexico. SAO and NCAR staff will reach out to US Embassy personnel to arrange tours of the GV and to give talks on eclipse science. In addition, the SAO team will reach out to their contacts at the University of Texas Rio Grande Valley about the possibility of a bilingual outreach event at their Brownsville campus.

Broadening STEM Participation of Underrepresented Groups: ACES is led by two women in early to mid-career STEM positions, Jenna Samra and Vanessa Marquez, who are well-placed to attract young women to STEM fields. Dr. Samra presented the AIR-Spec science and instrument development at an Astronomy Club meeting at the Montrose School (an all-girls high school in Medfield, MA), and several students later visited SAO for a lab tour that highlighted AIR-Spec. Both Ms. Marquez and Dr. Samra described their eclipse experience and their paths to STEM careers at a meeting of Innovators for Purpose, a Cambridge-based group that seeks to interest students from under-resourced communities in science and technology. ACES will provide many opportunities to engage in outreach with these and other groups.

E. Management Plan

ACES takes the same approach to management as the successful AIR-Spec and ASPIRE projects. The schedule and risk mitigation strategy are informed by the team's experience designing three prior airborne

eclipse missions. The team members have expertise in solar physics, optical design, mechanical engineering, software development, data analysis, and project management, as well as strong working relationships forged during the development of AIR-Spec and ASPIRE.

E.1. Team Member Roles

The ACES team consists of the PI, four Co-PIs, and two visiting scientists. Dr. Jenna Samra, the PI, will oversee the project, develop the optical design, and lead the optical alignment, calibration, and testing efforts to ensure that ACES meets its science requirements. Co-PI and Lead Engineer Ms. Vanessa Marquez will lead the ACES mechanical design and construction and its integration with ASPIRE and the GV. Co-PI and Project Manager Mr. Peter Cheimets will track the instrument development progress and will be available as a resource to Ms. Marquez as she leads the engineering effort. Co-PI Dr. Chad Madsen will lead the ACES science effort, including development of the calibration pipeline and plasma data products. Co-PI Dr. Edward DeLuca will use his previous experience as the AIR-Spec PI to facilitate the science effort and will lead observation and coordination planning. Dr. Giulio Del Zanna, a visiting scientist from the University of Cambridge, will consult on the atomic physics required to interpret observations. Dr. Jonathan Franklin, a visiting scientist from Harvard University who has extensive experience making atmospheric measurements with a Bruker FTS, will guide the team in FTS operation and data reduction.

E.2. Schedule

The ACES development process will begin with the acquisition of the commercially available Bruker FTS mentioned in Section C.2. In the first year of the project, we will test this instrument on the ground and in flight. The lessons learned will inform our design of ACES, which will be developed and tested in the second and third years. ACES will be flight tested 4–5 months before the eclipse, leaving time for modifications if needed. Major stages in the development of ACES are shown in the schedule in Figure 14 and detailed below.

	Y1 (8/21–7/22)				Y2 (8/22–7/23)				Y3 (8/23–7/24)			
	Q1	Q2	Q3	Q4	Q1	Q2	Q3	Q4	Q1	Q2	Q3	Q4
Start (8/2/2021)	◆											
Spec & purchase Bruker	◆	◆	◆									
Assemble & test Bruker					◆	◆						
Design/build/test ACES					◆	◆	◆	◆				
Possible modifications									◆	◆		
Eclipse campaign										◆	◆	
Data reduction										◆	◆	
End (7/31/2024)												◆

Figure 14. Schedule for the development of ACES.

Aug. 2021 – Mar. 2022: Bruker FTS specification and purchase. We will specify the Bruker FTS, purchase it, and design all of the associated equipment necessary to use it to make observations of the sun. Much of this period (16 weeks) will be spent waiting for the FTS to be delivered. During the wait, we will purchase and fabricate the other items necessary for testing it.

Mar. 2022 – Jun. 2022: Bruker FTS assembly and testing. The Bruker FTS will be integrated with the ASPIRE optical feed infrastructure. The system will be tested in the lab, moved outside to observe the sun, and finally boxed and shipped to Colorado, where it will be mounted on the GV and tested in flight.

Jun. 2022 – Nov. 2023: ACES fabrication, alignment and testing. ACES will be designed in response to the findings from the Bruker tests, and the bulk of the instrument will be fabricated/purchased, aligned, and tested. (The purchase of the IR camera will be initiated in December 2021 because the camera’s design is fixed and its lead time is 10 months.) Once the system is complete, we will ship it to Colorado and flight test it on the GV. If issues come up in testing, we will make adjustments before the April 2024 eclipse.

Mar. 2024 – Apr. 2024: ACES eclipse campaign. The integrated system consisting of ACES and ASPIRE will be shipped to Colorado, uploaded onto the Gulfstream V, tested, and then flown into the eclipse on April 8. With the completion of the eclipse flight, the system will be shipped back to Cambridge, MA, where it will be available for any post-flight calibrations required during the data reduction process.

Apr. 2024 – Jul. 2024: Data reduction, papers and public outreach. The remainder of the project will be spent reducing the data and preparing publications on the results. Once this phase is complete, we will deliver the eclipse instrument to HAO.

E.3. Risk Mitigation

The development of ACES is gated by the immovable 2024 eclipse. Fortunately, the ACES team has successfully produced complex instrumentation for three different eclipses and is familiar with this unique form of schedule pressure. The key to meeting the eclipse deadline is to understand the instrument components at the start of the project, solidify the specifications for the longest lead and most complex items early on, and order or fabricate them as soon as possible. For ACES, this includes Bruker FTS, the IR camera, and some of the optics. We will complete the integral portions of the instrument (e.g. the vacuum chamber) as early in the development as possible. Once the long lead items have been received and are working, and the integral portions of the instrument are assembled, aligned and tested, we will focus on the portions of the instrument that enhance its performance.

ACES incorporates designs, components and processes that we have used successfully in the past. For example, the vacuum chamber design draws heavily on the design of the AIR-Spec cryostat, and the IR camera is very similar to the AIR-Spec camera. Wherever possible, we will simplify the system design and the procedures required to operate it to ensure that there are no mistakes.

The risk of single-point component failures is significantly mitigated by use of the AIR-Spec and ASPIRE equipment as spares. We have spares for the flight computer, real-time computer, and image stabilization camera. Spares will be shipped to the eclipse in the event a last-minute replacement is needed.

E.4. Instrument Facility and Operation

Once ACES has been commissioned, it will reside at NCAR HAO in Boulder, CO. When in use, it will be mounted on the GV aircraft in nearby Broomfield. ACES will use liquid nitrogen to maintain its internal temperature; other than that, it uses no consumables beyond electric power.

HAO and NCAR, with consultation from SAO, will be responsible for scheduling the use of ACES once they take delivery. HAO and NCAR have broad experience supporting guest usage of existing telescopes and instrumentation. Standing allocation committees will be used to review reuse proposals. Coordination of requests with Earth Observing Laboratory (operators of the NCAR HIAPER GV aircraft) will be handled by HAO. HAO will solicit proposals for the use of ACES within the solar community. The SAO team will be available for advice and consultation as requested by HAO. ACES will join the AIR-Spec cryogenic spectrometer, the new narrowband imager and ASPIRE in the constellation of instruments that SAO has successfully developed when they are delivered.

E.5. Budget Materials and Cost Estimates

The equipment and materials in the budget will be used to build the ACES instrument. A detailed breakdown is given in the budget justification. All costs are based on vendor quotes or catalog list prices.

E.6. Design Distribution

SAO has a mission to disseminate knowledge and advance understanding through research and education. To this end, the ACES instrument design will be published in a refereed paper and presented at an engineering conference (e.g. SPIE), and the investigators will share design details with any group that requests them.

References

- [1] M. Asplund, N. Grevesse, A. J. Sauval, and P. Scott. The Chemical Composition of the Sun. *Annu. Rev. Astron. Astrophys.*, 47(1):481–522, Sept. 2009. doi: 10.1146/annurev.astro.46.060407.145222.
- [2] C. L. Bennett, M. R. Carter, D. J. Fields, and J. A. M. Hernandez. Imaging fourier transform spectrometer. In *Imaging Spectrometry of the Terrestrial Environment*, volume 1937, pages 191–200. International Society for Optics and Photonics, 1993.
- [3] E. Cervantes Alcala, G. Guth, S. Fedeler, J. Samra, P. Cheimets, E. DeLuca, and L. Golub. Development of the User Interface for AIR-Spec. In *AGU Fall Meeting Abstracts*, pages SM51A–2458, Dec. 2016.
- [4] G. Del Zanna and E. E. DeLuca. Solar coronal lines in the visible and infrared: A rough guide. *The Astrophysical Journal*, 852(1):52, 2018. URL <https://doi.org/10.3847/1538-4357/aa9edf>.
- [5] G. Del Zanna and H. E. Mason. Solar UV and X-ray spectral diagnostics. *Living Reviews in Solar Physics*, 15(1):5, Aug. 2018. doi: 10.1007/s41116-018-0015-3.
- [6] G. Del Zanna, P. J. Storey, N. R. Badnell, and V. Andretta. Helium Line Emissivities in the Solar Corona. *Astrophys. J.*, 898(1):72, July 2020. doi: 10.3847/1538-4357/ab9d84.
- [7] K. P. Dere, G. Del Zanna, P. R. Young, E. Landi, and R. S. Sutherland. CHIANTI—An Atomic Database for Emission Lines. XV. Version 9, Improvements for the X-Ray Satellite Lines. *Astrophys. J. Supp. Series*, 241(2):22, Apr. 2019. doi: 10.3847/1538-4365/ab05cf.
- [8] M. A. Duvernois and M. R. Thayer. The Elemental Composition of the Galactic Cosmic-Ray Source: ULYSSES High-Energy Telescope Results. *Astrophys. J.*, 465:982, July 1996. doi: 10.1086/177483.
- [9] C. B. Farmer and R. H. Norton. A high-resolution atlas of the infrared spectrum of the sun and the earth atmosphere from space. A compilation of ATMOS spectra of the region from 650 to 4800 cm⁻¹ (2.3 to 16 μm). Vol. I. The sun. Technical Report RP-1224, National Aeronautics and Space Administration, 1989.
- [10] S. Fedeler, J. Samra, and G. Guth. Development of Real-Time Image Stabilization for an Airborne Infrared Spectrometer. In *American Astronomical Society Meeting Abstracts #229*, volume 229 of *American Astronomical Society Meeting Abstracts*, page 437.02, Jan. 2017.
- [11] J. Geiss, G. Gloeckler, R. von Steiger, H. Balsiger, L. A. Fisk, A. B. Galvin, F. M. Ipavich, S. Livi, J. F. McKenzie, K. W. Ogilvie, and B. Wilken. The Southern High-Speed Stream: Results from the SWICS Instrument on Ulysses. *Science*, 268(5213):1033–1036, May 1995. doi: 10.1126/science.7754380.
- [12] P. R. Griffiths and J. A. De Haseth. *Fourier transform infrared spectrometry*, volume 171. John Wiley & Sons, 2007.
- [13] S. R. Habbal, M. Druckmüller, H. Morgan, A. Ding, J. Johnson, H. Druckmüllerová, A. Daw, M. B. Arndt, M. Dietzel, and J. Saken. Thermodynamics of the solar corona and evolution of the solar magnetic field as inferred from the total solar eclipse observations of 2010 July 11. *The Astrophysical Journal*, 734(2):120, 2011. URL <https://doi.org/10.1088/0004-637X/734/2/120>.

- [14] P. Judge, B. Berkey, A. Boll, P. Bryans, J. Burkepile, P. Cheimets, E. DeLuca, G. de Toma, K. Gibson, L. Golub, J. Hannigan, C. Madsen, V. Marquez, A. Richards, J. Samra, S. Sewell, S. Tomczyk, and A. Vera. Solar Eclipse Observations from the Ground and Air from 0.31 to 5.5 Microns. *Solar Phys.*, 294(11):166, Nov. 2019. doi: 10.1007/s11207-019-1550-3.
- [15] P. G. Judge. Spectral lines for polarization measurements of the coronal magnetic field. I. Theoretical intensities. *The Astrophysical Journal*, 500:1009–1022, 1998. URL <https://doi.org/10.1086/305775>.
- [16] C. Kay and N. Gopalswamy. Using the Coronal Evolution to Successfully Forward Model CMEs’ In Situ Magnetic Profiles. *Journal of Geophysical Research (Space Physics)*, 122(12):11,810–11,834, Dec. 2017. doi: 10.1002/2017JA024541.
- [17] E. K. J. Kilpua, N. Lugaz, M. L. Mays, and M. Temmer. Forecasting the Structure and Orientation of Earthbound Coronal Mass Ejections. *Space Weather*, 17(4):498–526, Apr. 2019. doi: 10.1029/2018SW001944.
- [18] J. R. Kuhn, M. J. Penn, and I. Mann. The Near-Infrared Coronal Spectrum. *Astrophys. J. Lett.*, 456: L67, Jan. 1996. doi: 10.1086/309864.
- [19] J. R. Kuhn, J. Arnaud, S. Jaeggli, H. Lin, and E. Moise. Detection of an Extended Near-Sun Neutral Helium Cloud from Ground-based Infrared Coronagraph Spectropolarimetry. *Astrophys. J. Lett.*, 667(2):L203–L205, Oct. 2007. doi: 10.1086/522370.
- [20] E. Landi, U. Feldman, and K. P. Dere. A Comparison between Coronal Emission Lines from an Isothermal Spectrum Observed with the Coronal Diagnostic Spectrometer and CHIANTI Emissivities. *Astrophys. J.*, 574(1):495–503, July 2002. doi: 10.1086/340837.
- [21] S. D. Lord. A new software tool for computing Earth’s atmospheric transmission of near- and far-infrared radiation. NASA Technical Memorandum 103957, Dec. 1992.
- [22] C. A. Madsen, J. E. Samra, G. Del Zanna, and E. E. DeLuca. Coronal Plasma Characterization via Coordinated Infrared and Extreme Ultraviolet Observations of a Total Solar Eclipse. *Astrophys. J.*, 880(2):102, Aug. 2019. doi: 10.3847/1538-4357/ab2b3c.
- [23] F. Magnant-Crifo. Absolute Abundances and Distribution of Material versus Density and Temperature in a Coronal Condensation. *Solar Phys.*, 39(1):141–151, Nov. 1974. doi: 10.1007/BF00154976.
- [24] H. E. Mason. The interpretation of the forbidden emission lines from a coronal condensation. *Monthly Notices of the Royal Astronomical Society*, 171:119–130, Apr. 1975. doi: 10.1093/mnras/171.1.119.
- [25] M. R. Menzel, J. Samra, V. Marquez, P. Cheimets, and E. DeLuca. Upgrading Stability of an Airborne Infrared Spectrometer (AIR-Spec) for Coronal Observations. In *AGU Fall Meeting Abstracts*, volume 2018, pages SH11C–2890, Dec. 2018.
- [26] J. C. Raymond, J. L. Kohl, G. Noci, E. Antonucci, G. Tondello, M. C. E. Huber, L. D. Gardner, P. Niccolosi, S. Fineschi, M. Romoli, D. Spadaro, O. H. W. Siegmund, C. Benna, A. Ciaravella, S. Cranmer, S. Giordano, M. Karovska, R. Martin, J. Michels, A. Modigliani, G. Naletto, A. Panasyuk, C. Pernechele, G. Poletto, P. L. Smith, R. M. Suleiman, and L. Strachan. Composition of Coronal Streamers from the SOHO Ultraviolet Coronagraph Spectrometer. *Solar Phys.*, 175(2):645–665, Oct. 1997. doi: 10.1023/A:1004948423169.

- [27] J. Samra, P. Cheimets, E. DeLuca, J. Galeros, T. Gauron, L. Golub, G. Guth, E. Hertz, P. Judge, S. Koutchmy, and V. Marquez. An airborne infrared spectrometer for solar eclipse observations. In C. J. Evans, L. Simard, and H. Takami, editors, *Ground-based and Airborne Instrumentation for Astronomy VI*, volume 9908 of *Proceedings of SPIE Astronomical Telescopes and Instrumentation*, page 99085U, 2016. URL <https://doi.org/10.1117/12.2232128>.
- [28] J. E. Samra, P. G. Judge, E. E. DeLuca, and J. W. Hannigan. Discovery of new coronal lines at 2.843 and 2.853 μm . *The Astrophysical Journal Letters*, 856(2):L29, 2018. URL <https://doi.org/10.3847/2041-8213/aab434>.
- [29] J. E. Samra, P. G. Judge, E. E. DeLuca, and J. W. Hannigan. Erratum: “Discovery of New Coronal Lines at 2.843 and 2.853 μm ” (2018, ApJL, 856, 129). *The Astrophysical Journal*, 873(2):L25, Mar 2019. doi: 10.3847/2041-8213/ab0ae0. URL <https://doi.org/10.3847/2041-8213/ab0ae0>.
- [30] P. Scott, M. Asplund, N. Grevesse, M. Bergemann, and A. J. Sauval. The elemental composition of the Sun. II. The iron group elements Sc to Ni. *Astron. Astrophys.*, 573:A26, Jan. 2015. doi: 10.1051/0004-6361/201424110.
- [31] P. Scott, N. Grevesse, M. Asplund, A. J. Sauval, K. Lind, Y. Takeda, R. Collet, R. Trampedach, and W. Hayek. The elemental composition of the Sun. I. The intermediate mass elements Na to Ca. *Astron. Astrophys.*, 573:A25, Jan. 2015. doi: 10.1051/0004-6361/201424109.
- [32] N. Tañón Reyes and C. Madsen. Total Solar Eclipse Science and Outreach in Perú. In *American Astronomical Society Meeting Abstracts #235*, volume 235 of *American Astronomical Society Meeting Abstracts*, page 239.07, Jan. 2020.
- [33] N. Tañón Reyes, J. Samra, C. Madsen, and E. DeLuca. Eclipse Results from the Airborne Infrared Spectrometer (AIR-Spec) and the Extreme-ultraviolet Imaging Spectrometer (EIS). In *American Astronomical Society Meeting Abstracts #235*, volume 235 of *American Astronomical Society Meeting Abstracts*, page 210.09, Jan. 2020.
- [34] A. Vira. Alignment and Calibration of an Airborne Infrared Spectrometer. In *AGU Fall Meeting Abstracts*, volume 2017, pages SH13B–2481, Dec. 2017.
- [35] A. Vira, J. Samra, P. Cheimets, E. DeLuca, S. Fedeler, G. Guth, and V. Marquez. Image stabilization for Airborne Infrared Spectrometer. In M. Strojnik and M. S. Kirk, editors, *Infrared Remote Sensing and Instrumentation XXVI*, volume 10765 of *Proceedings of SPIE Optics and Photonics*, page 107650J, 2018. URL <https://doi.org/10.1117/12.2319890>.
- [36] A. Vourlidas, S. Patsourakos, and N. P. Savani. Predicting the geoeffective properties of coronal mass ejections: current status, open issues and path forward. *Philosophical Transactions of the Royal Society of London Series A*, 377(2148):20180096, July 2019. doi: 10.1098/rsta.2018.0096.
- [37] L. Wallace, W. Livingston, K. Hinkle, and P. Bernath. Infrared Spectral Atlases of the Sun from NOAO. *Astrophys. J. Supp. Series*, 106:165, Sept. 1996. doi: 10.1086/192333.
- [38] R. D. V. R. Woolley and C. W. Allen. The Coronal Emission Spectrum. *Monthly Notices of the Royal Astronomical Society*, 108:292, Jan. 1948. doi: 10.1093/mnras/108.3.292.